Transient and sustained visuomotor selection during working-memory guided behavior.

Edward F. Ester[1,2], Rachel Weese[1]

[1]Department of Psychology, University of Nevada, Reno
[2]Integrative Neuroscience Program, University of Nevada, Reno

Support: NSF 2050833 (E.F.E.), Nevada Undergraduate Research Award (R.W.)

Contributions: E.F.E. and R.W. conceived and designed the experiment. R.W. collected data, E.F.E. and R.W. analyzed data. E.F.E. and R.W. wrote the manuscript.

Data and Analytic Software: forthcoming!

Abstract

Many recent studies have documented links between circuit-, network-, and brain-level mechanisms supporting the initiation of working memory-guided behaviors. However, few have examined how sensorimotor representations stored in working memory are used to plan *future* behaviors. We leverage the high temporal resolution of human EEG recordings to show that when planning future memory-guided behaviors the brain switches from an initial joint visuomotor code to a subsequent motor-only code.

Memory-guided behaviors require the efficient selection of task-relevant mnemonic representations and motor plans. This is particularly important in the case of working memory (WM), a short-duration, capacity-limited system that forms a temporal bridge between fleeting sensory phenomena and possible actions (1-2). Recent studies in humans, nonhuman primates, and rodents suggest a tight coupling between brain networks and circuits that control access to the contents of WM and those that control access to possible actions (3-14). Complementary studies suggest that the human brain stores representations of sensory stimuli and prospective action plans in WM (15-18) and can select task-relevant mnemonic and action representations in parallel to support rapid and efficient memory-guided behaviors (15).

Considerably less is known about visuomotor representations are used to plan *anticipated* actions required by many everyday tasks (e.g., the sequential steps needed to make your perfect cup of coffee or prepare your favorite meal). Once a desired goal state becomes obvious, what happens to visuomotor representations stored in WM? One possibility is that visuomotor representations are selected and prioritized until a prospective action is executed or completed, enabling precise and continuous memory-guided control of behavior. A second possibility is that visuomotor representations are selected and transformed into a prospective action plan based on the most likely response, freeing mnemonic resources for the processing of other stimuli and/or the preparation of other actions (e.g., 16-17).

We tested these alternatives by recording EEG from a custom montage (Fig S1) while 31 human volunteers performed a retrospectively cued orientation memory task (Fig 1a). Participants remembered the orientations of two gratings over a blank delay. 1.5 sec after encoding, a 100% valid color cue indicated which of the two gratings would be probed for report at the end of the trial and which hand should be used for memory recall (i.e., left or right; response hand/cue color mappings were counterbalanced across participants). A response display containing a vertically oriented grating was presented 1.0 seconds later; participants adjusted the orientation of this probe to match the orientation of the grating held in memory using the cued response hand. Participants performed this task well, recalling the orientation of the probed grating with an average (±1 S.E.M.) absolute error of 13.6° ± 0.75° and responded with the correct hand on 93.8% ± 0.89% of trials. Due to a coding error, we were unable to estimate stable response times (i.e., elapsed time between the onset of the probe display and an initial button press) for any of the 31 participants.

Following earlier work (15), we independently manipulated the physical location of the cue-matching stimulus (i.e., left vs. right visual field) and the cued response hand (i.e., left vs. right). This allowed us to characterize neural signals associated with the selection of visual and motor information in trial-averaged EEG data independently of any signal mixing or volume conduction. Moreover, our task allowed us to probe the dynamics of visuomotor selection during development of a *planned* action: upon presentation of retrocue display participants were free to select task-relevant visuomotor representations stored in WM but could not execute a response until one second later.

We considered three alternative models for prospective visuomotor selection (Fig. 1b-d). In the first model, the brain selects task-relevant visuomotor representations shortly after cue onset and these representations remain prioritized until a response is executed or completed (Fig 1b). In the second model, the selection of task-relevant

visuomotor representations is delayed until the response period is imminent or has begun (Fig 1c). In the third model, the brain selects task-relevant visuomotor representations shortly after cue onset but transitions to a prospective motor-only code prior to probe onset (Fig 1d). All three of these models could be reconciled with prior results documenting the parallel selection of task-relevant visual and motor representations stored in WM (e.g., 15). However, only the third model predicts a transformation from a joint visuomotor to a later motor-only response code.

To evaluate these models, we used EEG to track neural signals associated with the selection of visual and motor information stored in memory in near-real-time (tens of milliseconds). We first identified EEG signals that co-varied with the physical location of the retrospectively cued stimulus (i.e., left vs. right visual hemifield; Fig 2a) and EEG signals that co-varied with the retrospectively cued response hand (i.e., left vs. right; Fig 2b). Because stimulus location and response hand were independently manipulated over trials (i.e., a stimulus requiring a right-hand response was equally likely to appear in the left vs. right visual field) we were able to characterize the selection of both attributes in trial-averaged EEG data independent one another. Thus, we attributed patterns of neural activity that covaried with stimulus location to the selection of visual information stored in WM and patterns of neural activity that covaried with response hand to the selection of motor information stored in WM.

Visual selection was associated with a robust but transient decrease in 8-13 Hz alpha power over electrode sites contralateral to the location of the cued stimulus (Fig 2a). This modulation was strongest over occipitoparietal electrode sites (Fig 2a; inset), consistent with prior reports linking changes in lateralized alpha power to shifts of attention in perception and working memory (15; 19-20). Conversely, motor selection was associated with a robust and sustained decrease in 8-13 Hz mu-alpha power and 15-30 Hz beta power over electrode sites contralateral to the location of the cued response hand (Fig 2b). This modulation was strongest over frontocentral electrode sites (Fig 2b; inset), consistent with prior reports linking changes in lateralized alpha power to shifts of attention in perception and working memory (15; 21). Direct comparisons of EEG signals associated with visual and motor selection are summarized in Fig 2c. Visual selection was transient, lasting approximately 300-900 ms after cue onset before returning to baseline. Conversely, motor selection began nearly concurrently with visual selection and persisted through the ensuring delay and response periods.

In a complementary analysis, we decoded the location of the retrospectively cued stimulus (i.e., left vs. right visual hemifield) and the retrospectively cued response hand (i.e., left vs right) from broadband (1-50 Hz) EEG responses measured over occipitoparietal and frontocentral electrode clusters where spectral signals associated with visual and motor selection were largest (occipitoparietal 10-20 electrode sites O1/2, PO3/4, PO7/8 and frontocentral 10-20 electrode sites C1/2 and C3/4; Fig 3c; qualitatively similar findings were obtained when decoding was based on all scalp electrode sites; Fig S2). This allowed us to probe task-relevant information in evoked (as compared to induced) EEG activity with an even greater temporal resolution (i.e., absent all but the most liberal spectral filters needed to remove low-frequency drifts and line noise from the EEG signal). We also attempted to decode the orientations of the

cued and uncued gratings but were unable to do so except during the probe period where a physical orientation was present on the screen (Fig S3).

Stimulus location decoding performance (i.e., left vs. right visual field) and response hand decoding performance (i.e., left vs. right hand) are summarized in Fig 3. A comparison of stimulus location and response hand decoding performance over occipitoparietal electrode sites (Fig 3a) revealed transient above-chance decoding of stimulus location during the delay separating the retrocue and probe displays. However, these effects were dwarfed by robust decoding of response hand over the cue-to-probe interval and during the response period. An identical analysis of stimulus location and response hand decoding performance over frontocentral electrode sites (Fig 3b) revealed a complementary pattern, with stimulus location decoding performance reaching above chance levels for a brief interval during the cue-to-probe delay and response hand decoding performance reaching above-chance levels during the cue-to-probe delay and during the response period. Note once again that these differences cannot be explained by volume conductance or signal mixing as we randomly and independently manipulated stimulus location and response hand over trials. Instead, they suggest that motor signals dominate memory signals when planning a future memory-guided behavior.

Memory systems are useful only insofar as they can be used to inform current and future actions. Although several recent studies have examined circuit-, network-, and brain-level interactions between WM and motor planning during overt action (3-18), few studies have examined the mechanisms responsible for *prospective* memory-guided actions. We leverage the high temporal precision of human EEG recordings to demonstrate that when planning a memory guided behavior the brain transitions from a visuomotor code to a motor-only code that persists until actions are executed (i.e., concurrent selection of visual and motor representations stored in memory followed by sustained selection of only motor representations; Fig 2C and Fig 3). This coding scheme has the advantage of freeing up mnemonic resources for the processing of other visual representations stored in WM and/or incoming sensory inputs that may be relevant to other future behaviors. Thus, our findings complement recent studies documenting intimate links between neural mechanisms of memory and motor control while revealing a novel mechanism for visuomotor transformations during planned memory-guided actions.

References

1. D'Esposito M, Postle BR. The cognitive neuroscience of working memory. Annual Review of Psychology, 66:115-142 (2015)

2. Buschman TJ. Balancing flexibility and interference in working memory. Annual Review of Vision Science, 7:367-388 (2021)

3. Chatham CH, Frank MJ, Badre D. Corticostriatal output gating during selection from working memory. Neuron 81:930-942 (2014)

4. Schneider D, Barth A, Wascher E. On the contribution of motor planning to the retroactive cuing benefit in working memory: Evidence by mu and beta oscillatory activity in the EEG. NeuroImage 162:73-85 (2017)

5. Wessel JR, Jenkinson N, Brittain J-S, Voets SHEM, Aziz TZ, Aron AR. Surprise disrupts cognition via a front-basal ganglia suppressive mechanism. Nature Communications 7:1-10 (2017)

6. Pho GN, Goard MJ, Woodson J, Crawford B, Sur M. Task-dependent representations of stimulus and choice in mouse parietal cortex. Nature Communications, 9:1-16 (2018)

7. Svoboda K, Li N. Neural mechanisms of movement planning: motor cortex and beyond. Current Opinion in Neurobiology, 49:33-41 (2018)

8. Minxha J, Adolphs R, Fusi S, Mamelak AN, Rutishauser U. Flexible recruitment of memory-based choice-representations by the human medial frontal cortex. Science, 368:eaba3313 (2020)

9. Tang C, Herikstad R, Parthasarathy A, Libedinsky C, Yen S-C. Minimally dependent activity subspaces for working memory and motor preparation in the lateral prefrontal cortex. eLife:9e58154 (2020)

10. Galero-Salas Y, Han S, Sych Y, Voigt FF, Laurenczy B, Gilad A, Helmchen F. Sensory and behavioral components of neocortical signal flow in discrimination tasks with short-term memory. Neuron, 109:135-148 (2021)

11. Rac-Lubashevsky R, Frank MJ. Analogous computations in working memory input, output and motor gating: Electrophysiological and computational modeling evidence. PLoS Computational Biology 17:e1008971 (2021)

12. Henderson MM, Rademaker RL, Serences JT. Flexible utilization of spatial- and motor-based codes for the storage of visuo-spatial information. eLife, 11:e75688 (2022)

13. Ariani G, Pruszynski JA, Diedrichsen J (2022) Motor planning brings human primary somatosensory cortex into action-specific prepatory states. eLife 11:e69517 (2022)

14. Kikumoto A, Mayr U, Badre D. The role of conjunctive representations in prioritizing and selecting planned actions. bioRxiv (2022)

15. van Ede F, Chekroud SR, Stokes M, Nobre AC. Concurrent visual and motor selection during visual working memory guided behavior. Nature Neuroscience, 22:477-483 (2019)

16. van Ede F, Deden J, Nobre AC. Looking ahead in working memory to guide sequential behavior. Current Biology 31:R779-R780 (2021)

17. van Ede F, Deden J, Nobre AC. Planning the potential future during multi-item visual working memory. bioRxiv (2021)

18. Boettcher SEP, Gresch D, Nobre AC, van Ede F. Output planning at the input stage in visual working memory. Science Advances 7:eabe8212 (2021)

19. van Ede F. Mnemonic and attentional roles for states of attenuated alpha oscillations in perceptual working memory: a review. European Journal of Neuroscience, 48:2509-2515 (2018)

20. Klimesch W. Alpha-band oscillations, attention, and controlled access to stored information. Trends in Cognitive Sciences, 16:606-617 (2012)

21. Jenkinson N, Brown P. New insights into the relationship between dopamine, beta oscillations, and motor function. Trends in Neurosciences, 34:611-618 (2018).

Supporting Online Methods

Research Participants. 32 human volunteers (both sexes) from the University of Nevada, Reno community completed a single 2.5-hour testing session in exchange for monetary remuneration ($15/h). All volunteers self-reported normal or corrected-to-normal visual acuity and gave both written and oral informed consent before enrolling in the study. Data from one participant who completed the study were excluded from final analyses due to chance-level task performance (i.e., the participant used the correct response hand on only 52% of trials); thus, the findings reported here reflect the remaining 31 participants.

Testing Environment. Participants were seated in a dimly lit room for the duration of testing. Visual displays were generated in MATLAB and rendered on a 27-inch LCD monitor (1920 x 1080 resolution) cycling at 240 Hz using Psychophysics Toolbox software extensions (22). Participants were seated approximately 80 cm from the display (head position was not constrained). Participants responded via buttons on a standard US computer keyboard.

Visuomotor Recall Task. A task schematic is shown in Figure 1A. Each trial began with a 500 ms sample display containing two colored gratings (radius 4.5° visual angle [DVA] from a viewing distance of 80 cm; 1.0 cycles/°) presented 7.0 DVA to the left and right of a central fixation point. The sample display was followed by a 1500 ms blank display and a 1000 ms retrospective cue display. The color of the retrospective cue instructed participants which grating would be probed at the end of the trial (i.e., blue or red) and which hand should be used to make a behavioral response (left or right). Cue-response mappings (i.e., red cue/left vs. right hand) were counterbalanced across participants. Each trial ended with a 2000 ms probe display containing a vertically oriented grating; participants recalled the orientation of the cued grating by adjusting the probe grating to match the corresponding sample grating using the cue-specific response hand. If participants were satisfied with their response before the end of the 2000 ms, they were instructed to refrain from pressing any other buttons. Participants completed 3 (N = 1), 7 (N = 2), or 8 (N = 28) blocks of 60 trials.

EEG Acquisition & Preprocessing. Continuous EEG was recorded from 63 scalp electrodes using a customized BrainProducts actiCHamp system using a left mastoid reference (10-20 electrode site TP9). Data were digitized at 1 kHz and later re-referenced to the algebraic mean of the left and right mastoids (using 10-20 site TP10 as the right mastoid reference). The following preprocessing steps were applied, in order: (1) resampling from 1 kHz to 500 Hz; (2) bandpass filtering from 1 to 50 Hz (zero-phase forward- and reverse- finite impulse response filters as implemented by EEGLAB software extensions; 23); (3) identification, removal, and reconstruction of noisy epochs via artifact subspace reconstruction (implemented via EEGLAB; 24-25), (4) epoching from -1.0 to +5.0 sec relative to the start of each trial, and (5) application of a surface Laplacian to remove low spatial frequency components from the signal (26).

Spectral Analyses. Spectral analyses focused occipitoparietal and frontocentral 10-20 electrode site pairs O1/2, PO3/4, PO7/8, C1/C2, and C3/C4; analyses were restricted to a period spanning -500 to +2500 ms before and after retrocue onset. We extracted broadband spectral power from each electrode on each trial using a short-time Fourier transform (STFT) with a frequency range from 1-40 Hz (in 0.25 Hz steps) using a 200 ms sliding window and 2 ms step size. Power was computed by squaring the absolute value of the complex Fourier coefficients within each STFT window.

To quantify changes in lateralized activity during visual selection, we sorted power estimates at each occipitoparietal electrode site by the location of the retrospectively cued stimulus, i.e., contralateral vs. ipsilateral hemifield, and expressed this difference as a normalized percentage:

$$L_i = 100 \times \frac{(c_i - s_i)}{(c_i + s_i)}$$

where c_i and s_i are the trial-averaged responses of electrode *i* when the retrospectively cued grating appeared in the contralateral or ipsilateral visual field, respectively. Lateralization estimates were pooled across occipitoparietal electrode sites, yielding a single time-frequency matrix of power estimates per participant. These matrices were averaged across participants to produce the data shown in Figure 2A.

An identical approach was used to quantify changes in lateralized activity during motor selection, with the exceptions that (a) analyses focused exclusively frontocentral electrode sites, and (b) trial-wise power estimates were sorted by the retrospectively cued response hand rather than stimulus location. This analysis was used to generate the data shown in Figure 2B.

To generate the topographical maps of alpha- and beta-band lateralization shown in Figures 2A and 2B, we repeated this analysis for every scalp electrode and averaged power estimates over 8-13 Hz (“alpha-band” activity) and 15-30 Hz (“beta-band” activity) over a period from 500-1000 Hz. These frequency bands were chosen a priori based on commonly reported values in the literature (e.g., 19, 21); this specific temporal window was chosen a priori based on prior reports suggesting that it takes human observers ~300-500 ms to process and respond to a retrospective memory cue (e.g., 27).

An analogous procedure was used to measure frontocentral beta-power lateralization, with the exceptions that (a) analyses focused on frontocentral electrode sites and (b) trial-wise recordings were sorted as contralateral or ipsilateral relative to the retrospectively cued response hand.

To visualize changes in occipitoparietal alpha power, frontocentral mu-alpha power, and frontocentral beta power (e.g, Fig 2C), we extracted and averaged lateralization estimates from 8-13 Hz over electrode sites O1/2, PO3/4, and PO7/8, lateralization

estimates from 8-13 Hz over electrode sites C1/2, C3/4, and lateralization estimates from 15-30 Hz over electrode sites C1/2, C3/4. Statistical analyses of lateralization were performed using nonparametric sign permutation tests with temporal cluster-based correction (see *Statistical Analyses*, below).

Decoding Analysis. Decoding analyses (Fig 3) were applied to broadband (1-50 Hz) signals measured at occipitopartietal electrode sites O1/2, PO3/4, PO7/8 and frontocentral electrode sites C1/2, C3/4. Decoding performance was computed separately for each time sample using 10-fold cross-validation. During each cross-validation fold, we designated 90% of available trials as a training data set and the remaining 10% of trials as a test data set, taking care to ensure that the training data set contained an equal number of observations for each possible outcome (e.g., for stimulus location decoding, we ensured that the training data set contained an equal number of left- and right visual field trials; likewise, for response hand decoding we ensured that the training data set contained an equal number of left- and right-hand trials). Decoding performance was computed by fitting a multivariate normal density to observations associated with each class in the training data set (using a pooled diagonal covariance matrix estimate), then assigning observations in the test data set to groups based on likelihood ratios. Qualitatively similar findings were obtained using other decoding approaches (e.g., using multivariate distance as in 28-29; Fig S4).

Decoding performance was quantified by computing the proportion of test trials where the classifier predicted the correct stimulus location or response hand. Performance estimates were averaged across cross-validation folds, yielding a single stimulus location and response hand decoding time series per participant and electrode cluster (i.e., occipitoparietal vs. frontocentral). Since stimulus location and response hand were binary variables, we evaluated decoding performance against a chance level of 50%.

Statistical Comparisons. All statistical comparisons reported here were based on nonparametric sign permutation tests (30). Specifically, each test we performed assumes a null statistic of 0 (i.e., no difference in alpha- or beta-band lateralization, or no difference in observed vs. chance decoding performance). We therefore generated null distributions of the differences between dependent variables (e.g., alpha- and beta-band lateralization, or location vs. response hand decoding) by randomly relabeling each participant's data with 50% probability and averaging the data across participants. This step was repeated 10,000 times, yielding a 10,000-element null distribution for each time point. Finally, we implemented a cluster-based permutation test with cluster-forming and cluster-size thresholds of $p < 0.05$ to evaluate differences with respect to this null distribution while correcting for multiple comparisons across time.

Online References

22. Kleiner M, Brainard D, Pelli D. What's new in Psychtoolbox-3? iPerception 36 (2007)

23. Delorme A, Makeig S. EEGLAB: An open-source toolbox for analysis of single-trial EEG dynamics including independent component analysis. Journal of Neuroscience Methods 134:9-21 (2004)

24. Chang C-Y, Hsu S-H, Pion-Tonachini L, Jung T-P. Evaluation of Artifact Subspace Reconstruction for automatic artifact components removal in multi-channel EEG recordings. IEEE Transactions on Biomedical Engineering, 67(4) (2019)

25. Blum S, Jacobsen NSJ, Bleichner MG, Debener S. A Reimannian modification of Artifact Subspace Reconstruction for EEG artifact handling. Frontiers in Human Neuroscience 141 (2019)

26. Perrin F, Pernier J, Bertrand O, Echallier JF. Spherical splines for scalp potential and current density mapping. Electroencephalography and Clinical Neurophysiology, 72:184-187 (1989)

27. Souza AS, Rerko L, Oberauer K. Unloading and reloading working memory: Attending to one item frees capacity. Journal of Experimental Psychology: Human Perception & Performance, 40:1237-1256 (2014)

28. Wolff MJ, Jochim J, Akyurek EG, Stokes MG. Dynamic hidden states underlying working-memory-guided behavior. Nature Neuroscience 20:864-871 (2017)

29. Wolff MJ, Kandemir G, Stokes MG, Akyurek EG. Unimodal and bimodal access to sensory working memories by auditory and visual impulses. Journal of Neuroscience, 40:671-681 (2020)

30. Maris E, Oostenveld R. Nonparametric statistical testing of EEG and MEG data. Journal of Neuroscience Methods, 164:177-190 (2007)

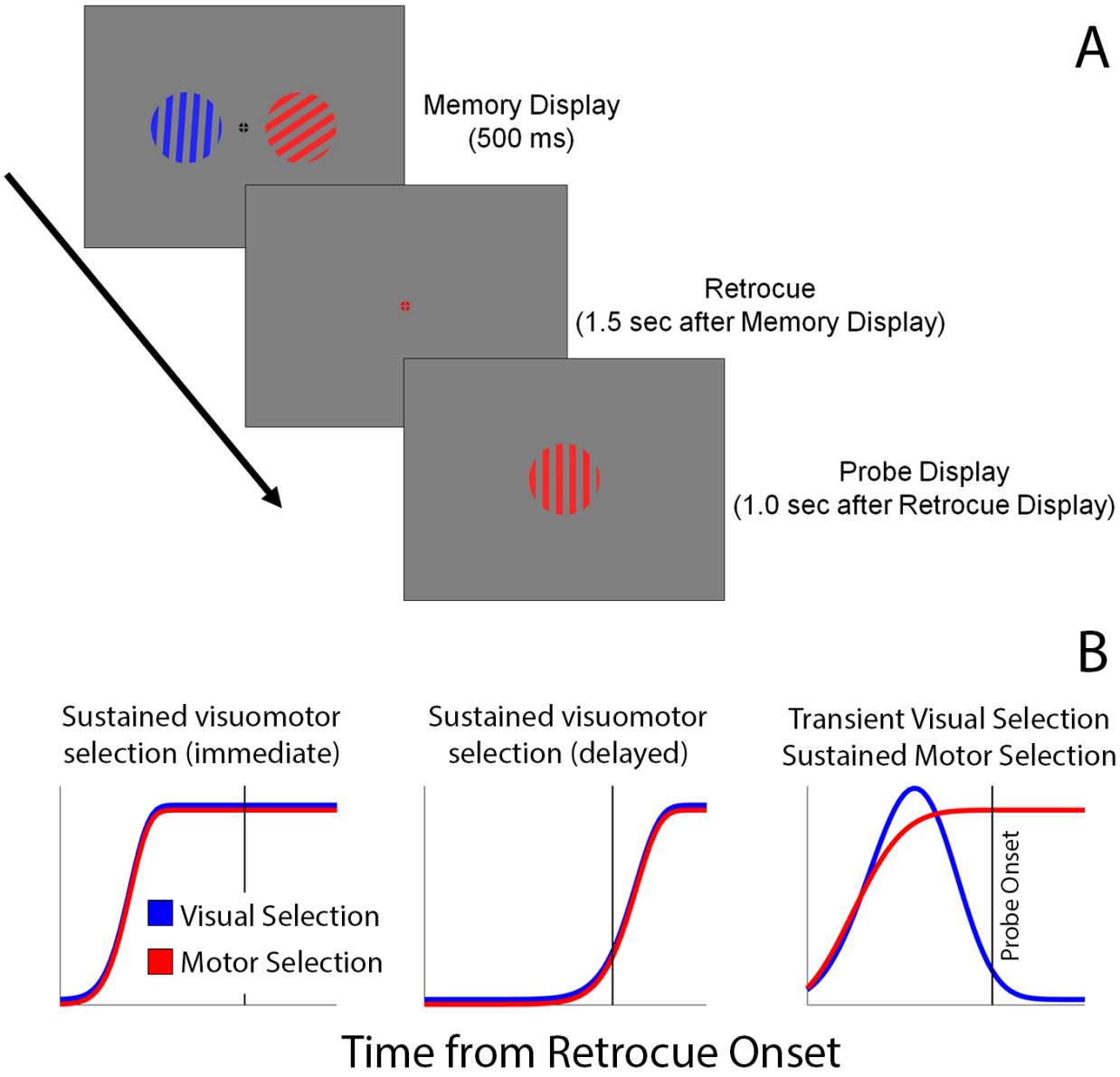

Fig. 1. Retrospectively Cued Visuomotor Selection Task and Possible Outcomes*. (a) Retrospectively cued orientation recall task. See text and Supporting Online Materials for more details. visual and motor selection. (b-d) Hypothetical time courses of visual and motor selection.*

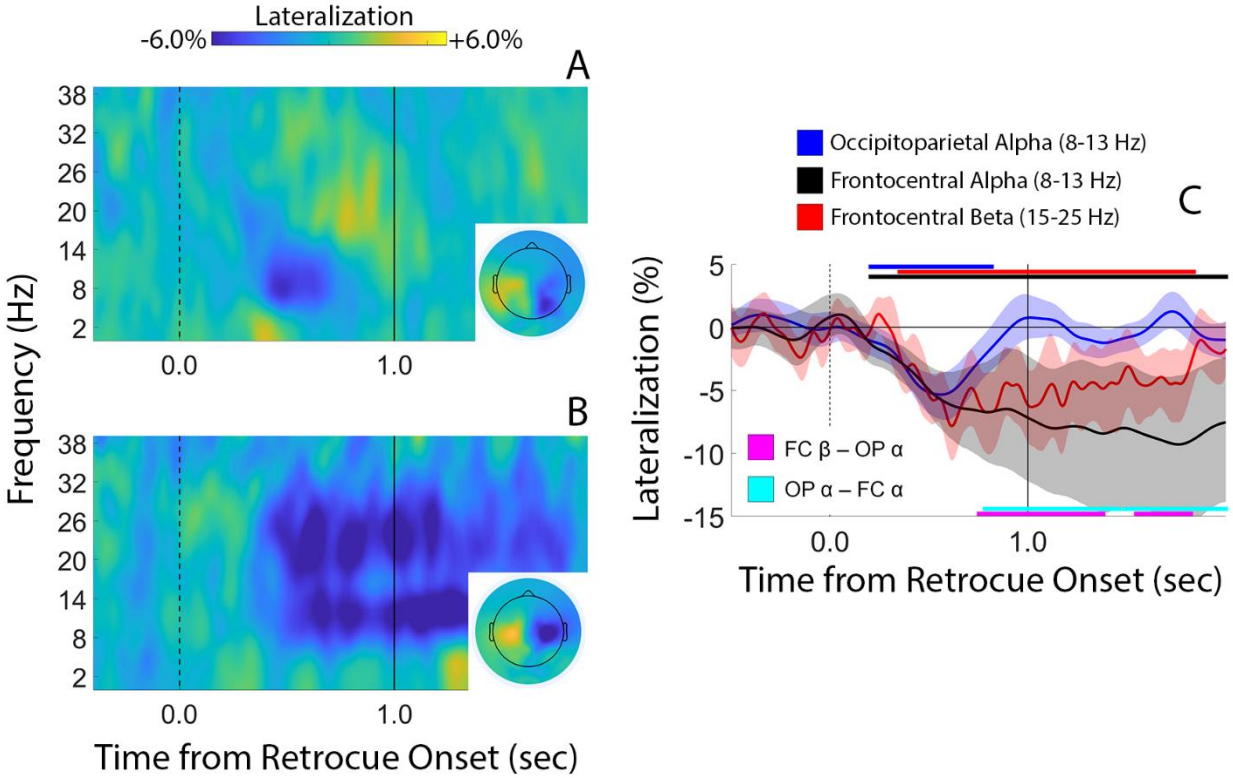

Fig. 2. Spectral signals associated with visual and motor selection during WM-guided behavior. *(a) Broadband frequency-specific lateralization over 10-20 occipitoparietal electrode site pairs O1/2, PO3/4, and PO7/8. Inset shows the distribution alpha-power lateralization (8-13 Hz) over all recorded electrode sites. (b) Broadband frequency-specific lateralization over 10-20 frontocentral electrode site pairs C1/2 and C3/4. Inset shows the distribution of beta-power lateralization (15-25 Hz) over all recorded electrode sites. (c) Occipitoparietal alpha-power (8-13 Hz) lateralization, frontocentral alpha-power lateralization, and frontocentral beta-power (15-25 Hz) time-locked to retrocue onset. Blue, red, and black bars at the top of the plot show periods where occipitoparietal/frontocentral lateralization was < 0. Maroon and cyan bars at the bottom of the plot show periods where frontocentral beta power was greater than occipitoparietal alpha power and frontocentral alpha power was greater than occipitoparietal alpha power, respectively. Shaded regions depict the 95% confidence interval of the mean. The vertical lines at time 0.0 and 1.0 depict the onset of the retrocue and probe displays, respectively.*

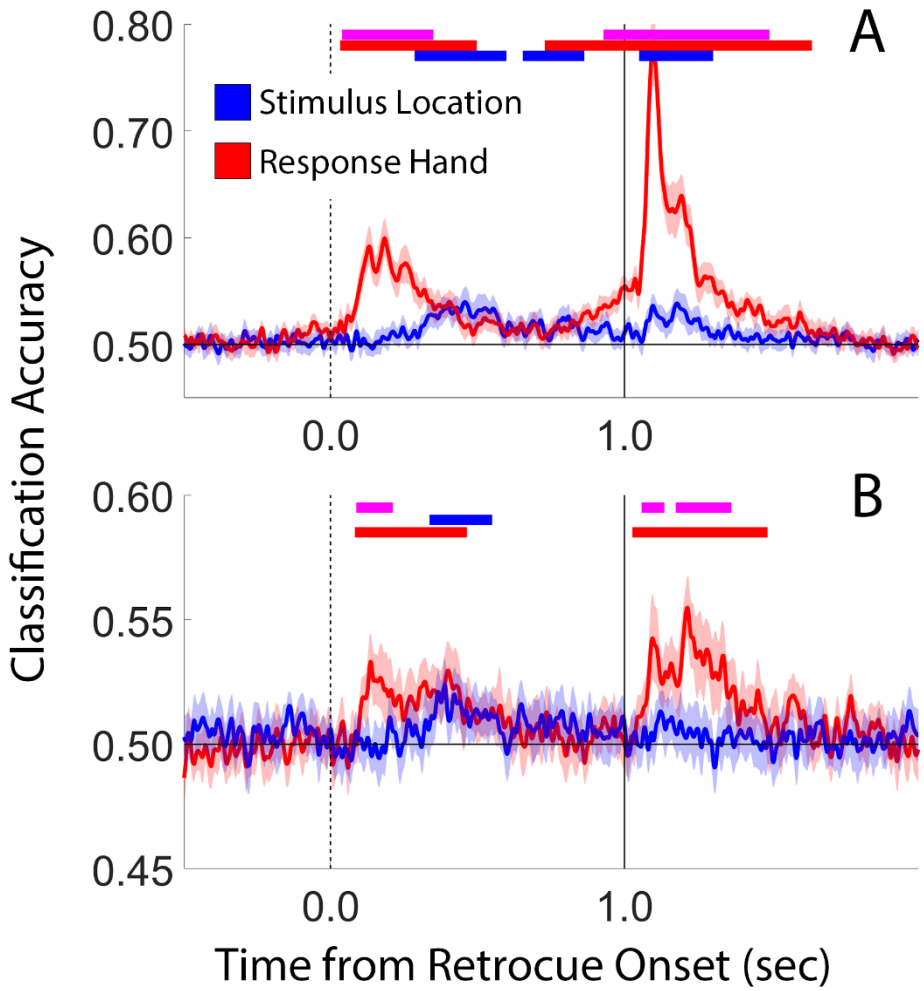

Fig 3. Location and Response Hand Decoding Performance in Occipitoparietal (a) and Frontocentral (b) Electrode Clusters. *We used a linear discriminant classifier (see Supporting Online Methods) to predict the location of the retrospectively cued grating (i.e., left vs. right visual field) and response hand (i.e., left vs. right hand) from broadband activity measured at occipitoparietal electrode clusters (O1/2, PO3/4, PO7/8; panel A) and frontocentral electrode clusters (C1/2, C3/4). Note that stimulus location and response hand were randomly and independently manipulated across trials; thus, similarities and/or differences in decoding performance across electrode clusters cannot be explained by volume conduction or signal mixing. Shaded regions around each line depict the 95% confidence interval of the mean. Blue and red bars at the top of each plot depict epochs where stimulus location and response hand decoding were significantly greater than chance (50%; nonparametric cluster-based permutation test; see Supporting Online Methods); maroon lines depict intervals where response hand decoding was significantly greater than stimulus location decoding. Vertical lines at time 0.0 and 1.0 depict the onset of the retrocue and probe displays, respectively.*